

Efficient Quantum Trace Estimation with Reconfigurable Real-Time Circuits

Yizhi Shen,^{1,*} Katherine Klymko,² Eran Rabani,^{3,4,5} Daan Camps,² Roel Van Beeumen,¹ and Michael Lindsey⁶

¹*Applied Mathematics and Computational Research Division,*

Lawrence Berkeley National Laboratory, Berkeley, CA 94720, USA

²*NERSC, Lawrence Berkeley National Laboratory, Berkeley, CA 94720, USA*

³*Materials Sciences Division, Lawrence Berkeley National Laboratory, Berkeley, CA 94720, USA*

⁴*Department of Chemistry, University of California, Berkeley, Berkeley, CA 94720, USA*

⁵*The Sackler Center for Computational Molecular and Materials Science, Tel Aviv University, Tel Aviv 69978, Israel*

⁶*Department of Mathematics, University of California, Berkeley, Berkeley, CA 94720, USA*

Recently, quantum algorithms that leverage real-time evolution under a many-body Hamiltonian have proven to be exceptionally effective in estimating individual eigenvalues near the edge of the Hamiltonian spectrum, such as the ground state energy. By contrast, evaluating the trace of an operator requires the aggregation of eigenvalues across the entire spectrum. In this work, we introduce an efficient near-term quantum algorithm for computing the trace of a broad class of operators, including matrix functions of the target Hamiltonian. Our trace estimator is similar to the classical Girard-Hutchinson estimator in that it involves the preparation of many random states. Although the exact Girard-Hutchinson estimator is not tractably realizable on a quantum computer, we can construct random states that match the variance of the Girard-Hutchinson estimator through only real-time evolution. Importantly, our random states are all generated using the same Hamiltonians for real-time evolution, with randomness owing only to stochastic variations in the duration of the evolutions. In this sense, the circuit is reconfigurable and suitable for realization on both digital and analog platforms. For numerical illustration, we highlight important applications in the physical, chemical, and materials sciences, such as calculations of density of states and free energy.

I. INTRODUCTION

Computing the trace of an operator is a task with wide-ranging applications across the mathematical and physical sciences [1–7]. Direct evaluation of the operator trace, though invariant under a basis rotation, involves repeated calculations of matrix-vector products. The number of calculations grows with the dimension of the underlying vector space. When the vector space is of high dimension, direct evaluation becomes prohibitively expensive.

To address this difficulty, stochastic trace estimators are commonly implemented [8–14]. Instead of computing the operator diagonal directly, stochastic methods replace the complete orthonormal basis with a stochastic resolution of the identity. One major advantage of these methods is that the statistical variance of the resulting trace estimator is independent of the operator dimension, so a desired accuracy can be achieved with a dimension-independent number of operator queries. Nevertheless, such methods still require us to store vectors of the same dimension as the operator. For operators on quantum many-body Hilbert spaces, where the dimension is exponentially large in the system size or number of particles, direct classical implementation of traditional stochastic trace estimators becomes quickly infeasible.

In this manuscript, we introduce a quantum algorithm for stochastic trace estimation with theoretically controlled variance that is optimal in a sense to be described below. To prepare random vectors (*i.e.*, wavefunctions), we only make use of real-time evolutions under a fixed

set of simple auxiliary Hamiltonians, where only the evolution durations are randomized (and moreover independent of the system size). Due to phase cancellation, these random vectors can yield a stochastic resolution of identity. Since the auxiliary Hamiltonians are fixed and only the evolution durations are randomized, we say that the circuit implementing our quantum trace estimator is *reconfigurable*. That is, on both practical digital and analog platforms, we only implement a single hardware-native circuit designed for iterative reuse each time the randomness is sampled.

Compared to other approaches for trace estimation, the strengths of our approach are that it (1) generates random states from simple real-time evolutions whose durations are randomized independently of the system size, (2) attains the exact same relevant statistical moments as the standard classical benchmark that struggles with exponentially large Hilbert spaces, and (3) significantly enhances practical near-term quantum efficiency, since it eliminates the overhead required for approaches that implement a distinct circuit for each sampling instance.

Note that we do not require unitarity of the operator whose trace is to be computed. More generally we can consider matrix functions $f(H)$ of a many-body Hamiltonian H . To address the difficulty posed by non-unitarity, we leverage real-time-evolution-based strategies. Specifically, we can employ approaches based on linear combinations of unitaries (LCU) [15] and quantum signal processing (QSP) [16, 17], both of which allocate at most a single ancilla qubit. Our complete approach to trace estimation can therefore be viewed in its entirety as a real-time paradigm, exploiting the computational power of quantum hardware while prioritizing resource efficiency. As

* yizhis@lbl.gov

recent advances enable Hamiltonian simulation at ever-decreasing costs, our approach can be adapted readily to both near-term and early fault-tolerant quantum devices.

The manuscript is organized as follows. In Section II, we examine the theoretical framework of stochastic trace estimation. We start with a comprehensive overview of conventional approaches. We then expand on the intuition that real-time evolution of randomized duration can yield a stochastic resolution of the identity. Finally we present a practical reconfigurable approach for stochastic trace estimation. In Section III, we control the variance of this practical estimator and detail its reconfigurable circuit representations on digital and analog platforms. In Section IV, we present a preliminary error analysis accounting for noisy quantum hardware. In Section V, we numerically demonstrate the effectiveness of our estimator on the density of states and free energy calculations. In Section VI, we conclude and summarize.

II. REVIEW OF CLASSICAL AND QUANTUM TRACE ESTIMATION

The trace of an operator $A : \mathbb{C}^N \rightarrow \mathbb{C}^N$ is the diagonal sum

$$\text{Tr}[A] = \sum_{n=0}^{N-1} \langle \psi_n | A | \psi_n \rangle, \quad (1)$$

where $\{|\psi_n\rangle\}_{n=0}^{N-1}$ is any chosen orthonormal basis. Each basis vector $|\psi_n\rangle$ contributes a distinct matrix-vector product, thus requiring N in total for a full deterministic trace calculation. For large-scale problems, stochastic techniques sidestep this scaling difficulty, potentially requiring only $O(1)$ matrix-vector products to achieve an estimate of fixed accuracy. In particular, the operator trace can be estimated using randomly sampled normalized vectors $|\chi\rangle \stackrel{\text{iid}}{\sim} p(|\chi\rangle)$ according to a distribution p that yields the stochastic resolution of identity,

$$\mathbb{E}[|\chi\rangle\langle\chi|] = \frac{1}{N}\mathbb{I}, \quad (2)$$

where \mathbb{I} is the identity operator. Then one can approximate

$$\frac{1}{N}\text{Tr}[A] = \mathbb{E}\text{Tr}[|\chi\rangle A |\chi\rangle] \approx \frac{1}{K} \sum_{k=1}^K \langle \chi_k | A | \chi_k \rangle, \quad (3)$$

where the first equality follows from the cyclic property of the trace. The number K of stochastic matrix-vector products required to achieve a given target accuracy can be controlled based on the variance of the random variable $\langle \chi | A | \chi \rangle$, *i.e.*, $\mathbb{E}|\langle \chi | A | \chi \rangle|^2 - |\mathbb{E}\langle \chi | A | \chi \rangle|^2$. For many important models, the distribution $p(|\chi\rangle)$ can be chosen such that this variance and therefore the required number K of matrix-vector products are independent of the problem dimension N .

How are the random vectors $|\chi\rangle$ to be sampled? Girard and Hutchinson [9, 18] proposed a simple yet remarkably effective approach in which the coefficients χ_n of $|\chi\rangle$ in an arbitrary fixed orthonormal basis are sampled independently and uniformly from $\{-1, +1\}$, *i.e.*, sampled i.i.d. from the Rademacher distribution. An alternative approach chooses χ_n to be sampled independently and uniformly from the complex unit circle $\{e^{i\theta} : \theta \in [0, 2\pi)\}$, *i.e.*, sampled i.i.d. from the unit circle with uniform random phases. To obey our convention in which the states $|\chi\rangle$ are normalized, in both constructions it is necessary to further divide all components by the normalizing constant \sqrt{N} . If A is complex symmetric (and indeed one often reduces to this case), the random phase approach minimizes the variance among all distributions with i.i.d. components [11], though we comment that for purely real classical calculations it is not favored because it requires complex arithmetic. From here on, we will refer to this random-phase-based approach as the Hutchinson estimator.

While these stochastic techniques are straightforward to implement, in classical computing paradigms they encounter a curse of dimensionality for quantum many-body systems as the size N of the vectors grows exponentially. Meanwhile, within quantum computing paradigms it is not feasible to efficiently sample wavefunctions with i.i.d. components in a computational basis. We will see that we can nonetheless ‘spoo’ the Hutchinson estimator by sampling random wavefunctions with components that are dependent in a computational basis but precisely match the variance of the optimal Hutchinson estimator.

Before further detailing our quantum algorithm for trace estimation and its strengths, we review the existing approaches in the quantum computing paradigm. The earliest approaches trace their origin to the one clean qubit model of computation [19], a computing paradigm on maximally mixed states. With an additional ancilla qubit in its pure state, the normalized trace $\frac{1}{N}\text{Tr}[A]$ of a unitary operator A can be regarded as a state overlap and estimated from ancilla measurements through Hadamard tests. To simulate the mixed state $\frac{1}{N}\mathbb{I}$, it is equivalent to uniformly sample the computational basis $\{|\psi_n\rangle\}_{n=0}^{N-1}$. In contrast to the Hutchinson estimator, the one clean qubit protocol during any stochastic iteration requires storing only $\mathcal{O}(\log_2 N)$ random bits, each realizing a single-qubit gate. However, the associated statistical error in this case falls far short of that of the Hutchinson estimator [12].

Recent efforts have led to more efficient quantum trace estimation by exploiting unitary designs capable of approximately sampling the Haar random states [20–24]. In particular, the unitary 2-design achieved by the Clifford group has been considered in the work [25], which in fact also proposes a classical approach with $\mathcal{O}(\text{polylog}_2(N))$ runtime and memory complexity for certain 2-local quantum partition functions.

Alternatively, the so-called diagonal designs, which relax the requirement of full Haar randomness, involve only the action of random diagonal gates on some specific ref-

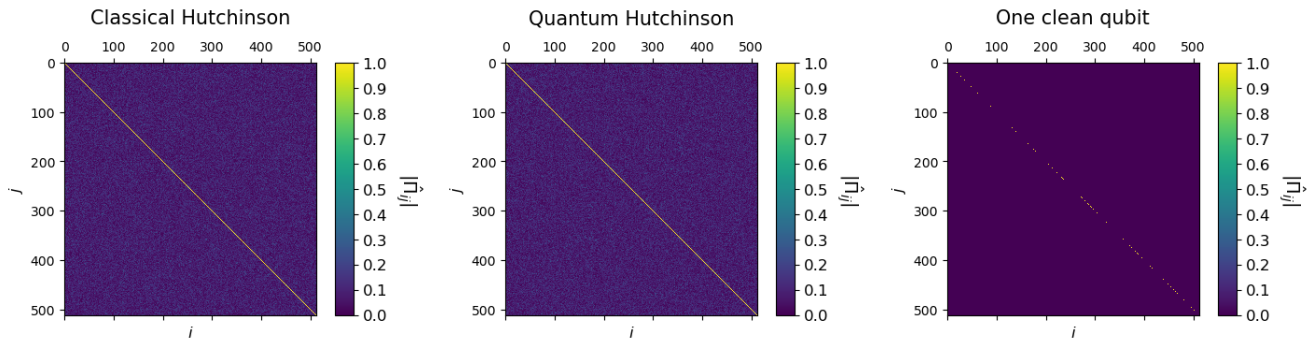


FIG. 1. Approximate resolution of identity $\hat{\Pi} = \frac{N}{K} \sum_{k=1}^K |\chi_k\rangle \langle \chi_k|$ constructed with $K = 10^2$ random states of various types. **Left:** Classical Hutchinson states. **Center:** Quantum Hutchinson states (this work). **Right:** Uniformly sampled computational basis, corresponding to the one clean qubit construction. Matrix elements $\hat{\Pi}_{ij}$ of the approximate identity operator are colored by their magnitudes. Color interpolates linearly from dark blue ($|\hat{\Pi}_{ij}| = 0$) to yellow ($|\hat{\Pi}_{ij}| = 1$).

reference state [26, 27], though to our knowledge the application to trace estimation has not been observed. In the context of unitary and diagonal designs, gate synthesis involves random draws from some pool of candidate operators, and this process typically requires us to construct a distinct circuit for each sampled random state. Despite encouraging theoretical guarantees such as a polynomial gate cost, such approaches would still be costly to implement on near-term quantum hardware, as the generation of random states requires manually executing the circuit compilations, each of varying gate composition and sequencing.

Finally, we highlight the QMETTS algorithm [28] as a quantum trace algorithm of important physical relevance. QMETTS is specifically designed for evaluating the ‘thermal expectations,’ *i.e.*, expressions of the form $\frac{\text{Tr}[Oe^{-\beta H}]}{\text{Tr}[e^{-\beta H}]}$ for some inverse temperature β and many-body Hamiltonian H . The key computational primitive in the algorithm (as in the original tensor-network based METTS algorithm [29]) is imaginary-time evolution, which may present more challenges than real-time based approaches on near-term hardware.

Our approach combines the strengths of classical and quantum stochastic trace estimators, with attention to minimal quantum resource constraints. The central ingredient is the stochastic real-time evolution of a single, easily prepared reference state, which yields random states achieving stochastic resolution of identity Eq. (2). Our approach can in fact be viewed as defining a diagonal 3-design, taking $\mathcal{O}(1)$ runtime and $\mathcal{O}((\log_2 N)^2)$ memory space. Importantly, this design is reconfigurable in the sense we have described above, distinguishing itself from the existing approaches, and moreover the construction is conceptually quite simple. With a short proof, we show that the statistical error of our estimator matches that of the Hutchinson estimator, which, as we have noted, is optimal among all estimators with independent components in the computational basis. The comparison is visualized in Fig. 1. We will therefore refer to our random

states as *quantum Hutchinson states*.

III. MAIN RESULTS

A. Quantum Hutchinson state construction

In this section we present the construction of our quantum Hutchinson states.

First we prepare the initial state of our circuit, which is a uniform superposition of the Z -computational basis elements $\vec{n} \in \{0, 1\}^Q$:

$$|\chi_0\rangle = |+\rangle^{\otimes Q} = \frac{1}{\sqrt{N}} \sum_{\vec{n} \in \{0, 1\}^Q} |\vec{n}\rangle, \quad (4)$$

with the use of $Q = \log_2 N$ Hadamard gates. Here Q denotes the number of qubits.

We evolve this initial state under the following diagonal Hamiltonian of spin-glass type:

$$G = \sum_{i \leq j}^Q \gamma_{ij} \Gamma_i \Gamma_j, \quad (5)$$

where $\Gamma_i = \frac{1-Z_i}{2}$ denotes the number operator acting on the qubit i , alternatively defined by $\Gamma_i |\vec{n}\rangle = n_i |\vec{n}\rangle$, and $\gamma_{ij} \sim \text{Uniform}(0, 2\pi)$ are independent and identically distributed random variables for all pairs of qubits $i \leq j$. We will evolve under G for one unit of time, and this action can be viewed as a sequence of real-time evolutions by all of the $\Gamma_i \Gamma_j$ (which all commute and hence do not introduce any Trotter error) for respective durations γ_{ij} . The quantum Hutchinson states are therefore sampled as

$$|\chi\rangle = e^{-iG} |\chi_0\rangle = \prod_{i \leq j}^Q e^{-i\gamma_{ij} \Gamma_i \Gamma_j} |\chi_0\rangle. \quad (6)$$

As a benchmark for comparison, we will also define the conventional Hutchinson state,

$$|\phi\rangle = \frac{1}{\sqrt{N}} \sum_{\vec{n}} e^{-i\theta_{\vec{n}}} |\vec{n}\rangle, \quad (7)$$

where $\theta_{\vec{n}} \sim \text{Uniform}(0, 2\pi)$ are independent and identically distributed random variables for all computational basis elements \vec{n} . We note that the conventional Hutchinson construction is *not tractably realizable on quantum hardware* but serves rather as an ideal standard for trace estimator variance.

B. Aside: construction with a single random time

As a theoretical question, it is interesting to consider whether it is possible to construct a suitable quantum Hutchinson state as $|\chi\rangle = e^{-iGt} |\chi_0\rangle$, where G is a single fixed Hamiltonian and t is a single random time. In fact, as we show in Appendix A, it is possible to achieve this goal where G is taken to be a linear combination of the diagonal operators Γ_i and $\Gamma_i\Gamma_j$. However, the random time t must be exponentially long in the number of qubits Q . Ultimately it is convenient to view such a long real-time evolution as a sequence of individual real-time evolutions, whose durations are drawn from a different joint distribution than that of our main construction, according to the Hamiltonian components Γ_i and $\Gamma_i\Gamma_j$. From this

point of view, the construction Eq. (6) emerges as a simpler alternative in which all the short random times are drawn independently. Moreover, the construction Eq. (6) enjoys the same hardware advantages of real-time evolution under a fixed set of elementary two-qubit Hamiltonians. Nonetheless, due to potential theoretical interest, we give further detail on the single-time construction in Appendix A, and we comment that in fact this work was initially motivated by this perspective.

C. Statistical properties

Now we show that the quantum Hutchinson state construction of Eq. (6) achieves the exact stochastic resolution of identity and thus yields unbiased trace estimates. Moreover, the variance matches that of the ideal Hutchinson estimator furnished by Eq. (7). Both statements are implied by the following theorem.

Theorem 1. Consider quantum Hutchinson and conventional Hutchinson states drawn randomly according to Eq. (6) and Eq. (7), respectively. The moments of these two constructions match up to third order in the sense that, for $d \leq 3$,

$$\mathbb{E} \left[(|\chi\rangle \langle \chi|)^{\otimes d} \right] = \mathbb{E} \left[(|\phi\rangle \langle \phi|)^{\otimes d} \right]. \quad (8)$$

Proof. We first observe that the Hutchinson construction admits the statistical moments

$$\mathbb{E} \left[(|\phi\rangle \langle \phi|)^{\otimes 1} \right] = \frac{1}{N} \sum_{\vec{n}} |\vec{n}\rangle \langle \vec{n}|, \quad (9)$$

$$\mathbb{E} \left[(|\phi\rangle \langle \phi|)^{\otimes 2} \right] = \frac{1}{N^2} \sum_{\substack{\vec{m}, \vec{m}', \vec{n}, \vec{n}': \\ (\vec{m}, \vec{m}') = \mathcal{P}_2(\vec{n}, \vec{n}') \text{ for some } \mathcal{P}_2 \in S_2}} |\vec{m}\vec{m}'\rangle \langle \vec{n}\vec{n}'|, \quad (10)$$

$$\mathbb{E} \left[(|\phi\rangle \langle \phi|)^{\otimes 3} \right] = \frac{1}{N^3} \sum_{\substack{\vec{m}, \vec{m}', \vec{m}'', \vec{n}, \vec{n}', \vec{n}''': \\ (\vec{m}, \vec{m}', \vec{m}'') = \mathcal{P}_3(\vec{n}, \vec{n}', \vec{n}''') \text{ for some } \mathcal{P}_3 \in S_3}} |\vec{m}\vec{m}'\vec{m}''\rangle \langle \vec{n}\vec{n}'\vec{n}''|, \quad (11)$$

where the $\mathcal{P}_d \in S_d$ appearing in the summations above indicate permutations of d binary vectors. The vector equality constraints up to permutation arise from the statistical independence of random phases $\theta_{\vec{n}}$ in Eq. (6).

Next we consider the quantum Hutchinson construction. Note that if $\gamma \sim \text{Uniform}(0, 2\pi)$, then for any integer k , the expectation $\mathbb{E}[e^{ik\gamma}]$ is one if $k = 0$ and zero otherwise. This identity enables the computations:

$$\mathbb{E} \left[(|\chi\rangle\langle\chi|)^{\otimes 1} \right] = \frac{1}{N} \sum_{\vec{m}, \vec{n}} \prod_{i \leq j}^Q \mathbb{E} \left[e^{i(n_i n_j - m_i m_j) \gamma} \right] |\vec{m}\rangle \langle \vec{n}|, \quad (12)$$

$$= \frac{1}{N} \sum_{\vec{m}, \vec{n}} \prod_{i \leq j}^Q \delta_{n_i n_j, m_i m_j} |\vec{m}\rangle \langle \vec{n}|, \quad (13)$$

$$= \frac{1}{N} \sum_{\substack{\vec{m}, \vec{n}: \\ \vec{m} \otimes \vec{m} = \vec{n} \otimes \vec{n}}} |\vec{m}\rangle \langle \vec{n}| \stackrel{\text{(Lemma 1)}}{=} \mathbb{E} \left[(|\phi\rangle\langle\phi|)^{\otimes 1} \right], \quad (14)$$

$$\mathbb{E} \left[(|\chi\rangle\langle\chi|)^{\otimes 2} \right] = \frac{1}{N^2} \sum_{\vec{m}, \vec{m}', \vec{n}, \vec{n}'} \prod_{i \leq j}^Q \delta_{n_i n_j + n'_i n'_j, m_i m_j + m'_i m'_j} |\vec{m}\vec{m}'\rangle \langle \vec{n}\vec{n}'|, \quad (15)$$

$$= \frac{1}{N^2} \sum_{\substack{\vec{m}, \vec{m}', \vec{n}, \vec{n}': \\ \vec{m} \otimes \vec{m} + \vec{m}' \otimes \vec{m}' = \vec{n} \otimes \vec{n} + \vec{n}' \otimes \vec{n}'}} |\vec{m}\vec{m}'\rangle \langle \vec{n}\vec{n}'| \stackrel{\text{(Lemma 1)}}{=} \mathbb{E} \left[(|\phi\rangle\langle\phi|)^{\otimes 2} \right], \quad (16)$$

$$\mathbb{E} \left[(|\chi\rangle\langle\chi|)^{\otimes 3} \right] = \frac{1}{N^3} \sum_{\substack{\vec{m}, \vec{m}', \vec{m}'', \vec{n}, \vec{n}', \vec{n}'': \\ \vec{m} \otimes \vec{m} + \vec{m}' \otimes \vec{m}' + \vec{m}'' \otimes \vec{m}'' = \vec{n} \otimes \vec{n} + \vec{n}' \otimes \vec{n}' + \vec{n}'' \otimes \vec{n}''}} |\vec{m}\vec{m}'\vec{m}''\rangle \langle \vec{n}\vec{n}'\vec{n}''| \stackrel{\text{(Lemma 1)}}{=} \mathbb{E} \left[(|\phi\rangle\langle\phi|)^{\otimes 3} \right]. \quad (17)$$

To arrive at Eqs. (14), (16) and (17) in the calculations, we have used the following lemma:

Lemma 1. For vectors $\vec{m}_1, \vec{m}_2, \vec{m}_3, \vec{n}_1, \vec{n}_2, \vec{n}_3 \in \{0, 1\}^Q$ and integer $1 \leq d \leq 3$, the matrix identity,

$$\sum_{i=1}^d \vec{m}_i \otimes \vec{m}_i = \sum_{i=1}^d \vec{n}_i \otimes \vec{n}_i, \quad (18)$$

holds if and only if $(\vec{m}_1, \dots, \vec{m}_d) = \mathcal{P}_d(\vec{n}_1, \dots, \vec{n}_d)$ for some permutation $\mathcal{P}_d \in S_d$. Here \otimes is understood as the vector outer product.

The proof of Lemma 1 is presented in Appendix B. This completes the proof of Theorem 1. \square

Now let us illustrate how Theorem 1 is applied to yield guarantees on our stochastic trace estimator $\langle\chi|A|\chi\rangle$ for $\frac{1}{N} \text{Tr}[A]$. First, the base case $d = 1$, together with Eq. (9), establishes the stochastic resolution of identity property, meaning that our estimator is unbiased. Second, we consider the case $d = 2$. Theorem 1 in this case, combined with Eq. (10), implies that

$$\mathbb{E} \left[(|\chi\rangle\langle\chi|)^{\otimes 2} \right] = \left(\frac{1}{N} \sum_{\vec{n}} |\vec{n}\rangle \langle \vec{n}| \right)^{\otimes 2} + \frac{1}{N^2} \sum_{\vec{m} \neq \vec{n}} |\vec{m}\vec{n}\rangle \langle \vec{n}\vec{m}|, \quad (19)$$

which recovers the well-known second moment of the Hutchinson estimator:

$$\mathbb{E} \left[|\langle\chi|A|\chi\rangle|^2 \right] = |\mathbb{E} \langle\chi|A|\chi\rangle|^2 + \frac{1}{N^2} \sum_{\vec{m} \neq \vec{n}} |\langle\vec{m}|A|\vec{n}\rangle|^2, \quad (20)$$

where $\mathbb{E} \langle\chi|A|\chi\rangle = \frac{1}{N} \text{Tr}[A]$.

Alternatively we can express the variance as

$$\mathbb{V} [\langle\chi|A|\chi\rangle] = \frac{1}{N^2} \sum_{\vec{m} \neq \vec{n}} |\langle\vec{m}|A|\vec{n}\rangle|^2 \leq \frac{1}{N^2} \|A\|_{\text{F}}^2, \quad (21)$$

where we have a succinct bound in terms of the Frobenius norm of the operator A . Note that the exact expression for the variance can often be reduced through similarity transformations, for example if A enjoys certain symmetries [30]. By Chebyshev's inequality, taking an empirical average over K random instances of our trace estimator as in Eq. (3), we expect that with high probability

$$\left| \frac{1}{K} \sum_{k=1}^K \langle\chi_k|A|\chi_k\rangle - \frac{1}{N} \text{Tr}[A] \right| \leq \frac{1}{N} \|A\|_{\text{F}} \epsilon, \quad (22)$$

where $\epsilon = \mathcal{O}(\frac{1}{\sqrt{K}})$ independently of A . In this sense, we say that the fluctuations of the estimator for the normalized trace are on the order of $\frac{1}{N} \|A\|_{\text{F}}$.

In the case where A is a positive semi-definite operator, which is of interest in the evaluation of a quantum partition function $\mathcal{Z} = \text{Tr}[A] = \text{Tr}[e^{-\beta H}]$, the trace bound $\|A\|_{\text{F}} \leq \text{Tr}[A]$ implies a bound (independent of A) on the relative error of the estimator with high probability. It is also interesting to consider the calculation of 'thermal expectations',

$$\langle O \rangle_H = \frac{\text{Tr}[O e^{-\beta H}]}{\text{Tr}[e^{-\beta H}]} = \frac{\frac{1}{N} \text{Tr}[O e^{-\beta H}]}{\frac{1}{N} \mathcal{Z}}, \quad (23)$$

where O is some observable of interest. Using Eq. (21), the standard deviation of the trace estimator for the nu-

merator can be bounded by

$$\frac{1}{N} \|Oe^{-\beta H}\|_F \leq \frac{1}{N} \|O\|_2 \|e^{-\beta H}\|_F \leq \frac{1}{N} \|O\|_2 \mathcal{Z}. \quad (24)$$

Hence if $\mathcal{Z} = \Omega(N)$, statistical fluctuations of the quotient of our numerator and denominator estimators are of order $\|O\|_2$, the operator norm of the observable, which is typically $\mathcal{O}(1)$ in the system size, *e.g.*, in the case of an average magnetization.

However, these comments regarding the partition function and thermal trace rely on a direct access to the operator exponential, which may be expensive on near-term hardware. In our numerical experiments, we will demonstrate how approaches fully based on real-time evolution are possible via the construction of the density of states. For the trace estimations required in these fully real-time approaches, A assumes the form of a unitary operator. In these cases, the fluctuations of the normalized trace are simply $\frac{1}{N} \|A\|_F = 1$.

D. Reconfigurability on digital platforms

Next we examine the hardware requirements for our estimator on a digital quantum platform. In particular, all quantum Hutchinson instances can be realized with a single reconfigurable quantum circuit.

Observe that by using $\Gamma_i \Gamma_j = \frac{1}{4}(1 - Z_i - Z_j + Z_i Z_j)$, the Hamiltonian G from Eq. (5) can be rewritten, up to a global phase, in terms of the Pauli Z operators as the Ising-type Hamiltonian,

$$G = \sum_{i<j}^Q h_{ij} Z_i Z_j + \sum_{i=1}^Q h_i Z_i, \quad (25)$$

with the Ising couplings and external field strengths given by $h_{ij} = \frac{\gamma_{ij}}{4}$ and $h_i = -\frac{\gamma_{ii}}{2} - \sum_{j>i} \frac{\gamma_{ij}}{4}$. The unitary time evolution in the Z -basis is hence a product of elementary diagonal gates,

$$e^{-iGt} = \left(\prod_{i \neq j}^Q e^{-ih_{ij} Z_i Z_j t} \right) \left(\prod_{i=1}^Q e^{-ih_i Z_i t} \right), \quad (26)$$

$$= \left(\prod_{i<j}^Q R_{zz}(4h_{ij}t|i, j) \right) \left(\bigotimes_{i=1}^Q R_z(2h_i t|i) \right), \quad (27)$$

where $R_z(\phi|i)$ and $R_{zz}(\phi|i, j)$ are one- and two-qubit Z -rotations of angle ϕ respectively. Each two-qubit rotation can be further unfolded as a CNOT-conjugated one-qubit rotation,

$$R_{zz}(\phi|i, j) = C_x(i, j) R_z(\phi|j) C_x(i, j), \quad (28)$$

where the CNOT, $C_x(i, j)$, acts on the control and target qubits (i, j) . Hence, the circuit can be efficiently synthesized using only one-qubit Z -rotations and two-qubit CNOT gates.

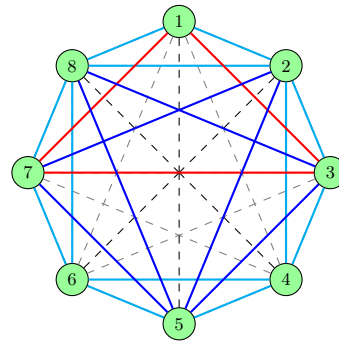


FIG. 2. Edge-disjoint triangles in a complete graph with $|\mathcal{V}| = Q = 8$ vertices. The colors distinguish triangles with different connectivities.

Notably, the quantum Hutchinson state sampling only involves modification of the $\mathcal{O}(Q^2)$ rotation angles but does not involve replacement or reordering of any gates. Moreover, by exploiting gate commutation relations, we can bound both the gate count and circuit depth required to produce a quantum Hutchinson state (cf. Theorem 2 below). The circuit we have presented yields a naïve gate count scaling of $\mathcal{O}(Q^2)$, with $\frac{Q(Q+1)}{2} R_z$ gates and $Q(Q-1)$ CNOT gates. While the implementation of this circuit is indeed feasible on devices with native all-to-all connectivity, we can slightly improve the naïve gate count and moreover show that the circuit depth is $\mathcal{O}(Q)$.

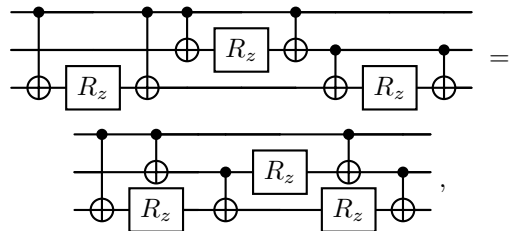
Theorem 2. e^{-iG} can be implemented using a single circuit with depth no greater than $D = 9Q - 2$, where the circuit contains $\frac{Q(Q+1)}{2} R_z$ gates and at most $N_{\text{CNOT}} = \lfloor \frac{5Q^2 - 3Q - 2}{6} \rfloor$ CNOT gates.

Proof. We exploit the commutation or rewriting rules for R_z and CNOT gates,

$$C_x(j, k) R_{zz}(\phi|i, j) = R_{zz}(\phi|i, j) C_x(j, k), \quad (29)$$

$$C_x(i, j) C_x(j, k) C_x(i, k) = C_x(j, k) C_x(i, j), \quad (30)$$

where (i, j, k) indexes a triplet of distinct qubit registries. When combined, the rules help improve local compilation as illustrated graphically below,



resulting in a reduction in both the gate count and circuit depth for a three-qubit block. Recall that each $R_{zz}(\phi|i, j)$ uniquely captures a two-body interaction $h_{ij} Z_i Z_j$ in G . So the overall resource reduction from our improved local compilation can be estimated by identifying the triplets

or triangles (i, j, k) that lack shared edges in an all-to-all graph representing our Ising Hamiltonian. This is a topic deeply examined in graph theory and combinatorics [31–33]. In particular, we highlight the fact that in a complete graph, $\mathcal{G} = (\mathcal{V}, \mathcal{E})$ with $|\mathcal{E}| = \frac{|\mathcal{V}|(|\mathcal{V}|-1)}{2}$, the maximal number of such edge-disjoint triangles is at least $N_a \geq \frac{(|\mathcal{V}|-1)(|\mathcal{V}|-2)}{6}$. For example, Fig. 2 shows the assembly of different three-qubit blocks in a 8-qubit complete graph, where a set of 7 edge-disjoint triangles is highlighted. The number of ‘dangling’ edges untouched by the triangles is therefore bounded by $N_b \leq |\mathcal{E}| - 3N_a = Q - 1$, which gives a total CNOT count of

$$N_{\text{CNOT}} \leq 5N_a + 2N_b. \quad (31)$$

Moreover, it is apparent that any two triangles commute with each other unless they share a common vertex. This observation allows us to bound the circuit depth,

$$D \leq 12 \lfloor \frac{Q}{2} \rfloor + 3N_b + 1, \quad (32)$$

where the first two terms in Eq. (32) account for the $\lfloor \frac{Q}{2} \rfloor$ layers of triangles with varying connectivities, as marked by the different colors in Fig. 2, and N_b layers of untouched dangling edges. We also include the layer of R_z gates that capture the external fields $\{h_i Z_i\}_{i=1}^Q$ in G .

(For the special cases $Q \equiv 1 \pmod{6}$ or $Q \equiv 3 \pmod{6}$, we saturate the optimal number of edge-disjoint triangles, $N_a = \frac{Q(Q-1)}{6}$. This implies a tighter bound of $N_{\text{CNOT}} \leq \frac{5Q^2-5Q}{6}$ and $D \leq 6Q + 1$ in these cases.) \square

E. Reconfigurability on analog platforms

In this section, we proceed to explore the hardware implementation of our estimator on a dynamics-driven analog platform, where the construction based on real-time evolution yields significant advantages. Our analysis primarily centers around systems of interacting neutral atoms undergoing Rydberg excitations. [34, 35] Though our focus is specific, similar considerations can hold for other analog models.

Recall that a general Rydberg Hamiltonian takes the form

$$G_{\text{Rydberg}} = \sum_{i=1}^Q \Omega_i X_i + \sum_{i=1}^Q \Delta_i \Gamma_i + \sum_{i < j}^Q V_{ij} \Gamma_i \Gamma_j, \quad (33)$$

where Ω_i and Δ_i determine the local Rabi frequency and detuning, respectively, on the atomic site i , while $V_{ij} \propto \frac{1}{r_{ij}^6}$ sets the repulsive van der Waals interaction between sites i and j separated by a distance of r_{ij} . Therefore our spin-glass Hamiltonian G is natively Rydberg with vanishing Rabi driving, $\Omega_i \equiv 0$.

In addition, preparation of the initial state can be accomplished by unit-time evolution under another Rydberg Hamiltonian of the form of Eq. (33), where $\Omega_i =$

$-\frac{\Delta_i}{2} = -\frac{\pi}{2\sqrt{2}}$ and $V_{ij} \equiv 0$. This is the case because

$$|\chi_0\rangle = \bigotimes_{i=1}^Q e^{i\frac{\pi}{2\sqrt{2}}(X_i+Z_i)} |\vec{0}\rangle, \quad (34)$$

where physical ground state $|\vec{0}\rangle$ is the native atomic configuration.

The overall evolution that we require, including the preparation of $|\chi_0\rangle$ can therefore be produced using the time-dependent waveforms,

$$\begin{cases} (\Omega_i, \Delta_i) = (-\frac{\pi}{2\sqrt{2}}, \frac{\pi}{\sqrt{2}}), & 0 \leq t \leq 1 \\ (\Omega_i, \Delta_i) = (0, \gamma_{ii}), & 1 \leq t \leq 2 \end{cases}, \quad (35)$$

prescribing piecewise-constant local Rabi drivings as well as detunings.

Moving forward, we discuss the simulation of the remaining pairwise coupling terms with physical interactions V_{ij} . Naïvely, given positive weights $\gamma_{ij} \stackrel{\text{iid}}{\sim} \text{Uniform}(0, 2\pi)$, we must choose the Q atomic positions \vec{r}_i so that the resulting distances $r_{ij} = \|\vec{r}_i - \vec{r}_j\|_2$ satisfy $V_{ij}(r_{ij}) = \gamma_{ij}$. However, this embedding problem is NP-hard when Q exceeds the spatial dimension (which is 3 at most), and valid solution does not exist in most cases.

Instead we formulate an alternative approach by exploiting the commutation of the diagonal operators Γ_i . As a first attempt we consider the decomposition $e^{-iGt} = \prod_{i < j} e^{-iG_{ij}t}$ where

$$G_{ij} := \gamma_{ij} \Gamma_i \Gamma_j + \frac{1}{Q-1} (\gamma_{ii} \Gamma_i + \gamma_{jj} \Gamma_j), \quad (36)$$

which holds because $\Gamma_i = \Gamma_i \Gamma_i$ for each i . The regrouping of the Hamiltonian contributions suggests that we should achieve the analog evolution e^{-iGt} using $\frac{Q(Q-1)}{2}$ analog blocks $e^{-iG_{ij}t}$ each of which couples only a single pair of atoms, and between which atom positions are dynamically shuffled.

However, by considering a more sophisticated coupling within each analog block we can bring the block depth down to Q . Theorem 3 below states this result and moreover quantifies the atom shuffling that we require between blocks in terms of the number of SWAP gates, each of which is realized as the physical swapping of a pair of atoms. In this construction, it is more convenient to work with simplified γ_{ij} that are sampled i.i.d. from the uniform distribution over the discrete set $\{0, \frac{2\pi}{3}, \frac{4\pi}{3}\}$. If γ is so distributed, then for any integer k , the expectation $\mathbb{E}[e^{ik\gamma}]$ is one if k is an integer multiple of 3 and zero otherwise. Therefore the variance equality from Theorem 1 holds just as well in this case.

Theorem 3. e^{-iG} can be implemented on a Rydberg simulator with at most Q analog blocks. Each of these analog blocks performs Rydberg evolution of time $\mathcal{O}(1)$ for a one-dimensional chain of Q Rydberg atoms. The circuit also involves a total of at most $N_{\text{SWAP}} = \frac{Q(Q-1)}{2}$

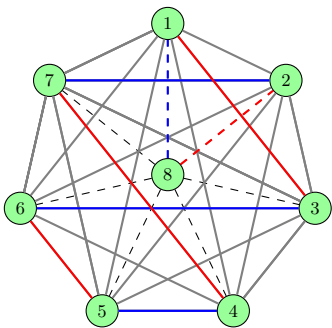


FIG. 3. Edge-coloring of a complete graph with $|\mathcal{V}| = Q = 8$ vertices. The colors partition all the edges into $(Q-1)$ groups. Each group represents a unique atom configuration consisting of disjoint doublets. For purpose of visualization, we highlight two of the colored groups (red and blue respectively).

SWAP gates, *i.e.*, the physical swaps of two atoms, which appear in between the analog blocks.

Proof. The use of the discrete couplings γ_{ij} allows us to consider only three physical distances $r_2 < r_1 < r_0$ such that $V_{ij}(r_2) = \frac{4\pi}{3}$, $V_{ij}(r_1) = \frac{2\pi}{3}$, and $V_{ij}(r_0) = 0$. This choice is possible owing to the rapid decay of the van der Waals interaction.

We now invoke classic edge coloring results for a complete graph of Q vertices corresponding to the Q qubits. Specifically, the edges of this graph can be decorated with at most Q different colors so that no incident edges have the same color. In general, edge colorings can be assigned efficiently with $\mathcal{O}(\text{poly}(Q))$ runtime [36, 37], but we make use of a very specific construction for the complete graph.

Without loss of generality, we assume that Q is even and use the following coloring. We distribute $Q-1$ vertices evenly on a circle to create a regular polygon and locate the remaining vertex at the center of the circle, as illustrated in Fig. 3. Then we assign a distinct color to each edge connecting a central-exterior vertex pair (as indicated by dashed lines in Fig. 3), and color the edges perpendicular to the central edge (as solid lines in Fig. 3). This assignment uses $\frac{|\mathcal{E}|}{|\mathcal{V}|/2} = Q-1$ colors to cover our complete graph.

Let $\{\mathcal{E}_i\}_{i=1}^{Q-1}$ be a partition of the edge set \mathcal{E} ,

$$\bigsqcup_{i=1}^{Q-1} \mathcal{E}_i = \mathcal{E}, \quad (37)$$

resulting from the coloring scheme above. Our analog evolution can thus be achieved using $Q-1$ blocks,

$$e^{-iG} = \prod_{k=1}^{Q-1} e^{-iG_k} = \prod_{k=1}^{Q-1} \prod_{(i,j) \in \mathcal{E}_k} e^{-iG_{ij}}, \quad (38)$$

where the Hamiltonian G_k for each analog block only includes interactions between atom dimers that share the same color assignment. The block Hamiltonian G_k can

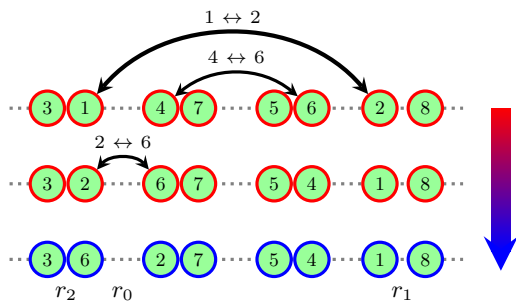


FIG. 4. Embedding of the edge-colored graph onto a 1D chain of interacting neutral atoms with $|\mathcal{V}| = Q = 8$ qubits. Each color, assigned on a subset of $Q/2$ edges, designates a dimer pairing of the vertices, which is reconfigured after each analog block e^{-iG_k} . The swapping involved in one such dimer reconfiguration (red to blue as in Fig. 3) is illustrated from top to bottom. The black bent arrows indicate the sequence of vertex transpositions needed to transition from the old to the new color assignment.

be embedded onto a one-dimensional lattice with variable lattice spacing r_0 , r_1 and r_2 as sketched in Fig. 4. To change the dimer configuration from G_k to G_{k+1} , we permute $Q/2$ vertices on the lattice since we can redistribute them to pair with the remaining half of the vertices. For example, the pairing $(3, 1) \mapsto (3, 6)$ in Fig. 4 from red to blue leaves the vertex 3 untouched. Such a permutation can be written as a sequence of at most $\frac{Q}{2} - 1$ elementary transpositions. A transposition of the two vertices i and j corresponds to the physical swapping of two atom positions. Such atom swaps upon the application of each analog block are shown schematically in Fig. 4. We notice that each set of $\frac{Q}{2}$ distinctly colored edges can be associated with one of the exterior edges $(1, 2), (2, 3), \dots$, etc. Since our graph of polygon exhibits a discrete rotational symmetry along its exterior edges, all the $|\mathcal{V}|$ edges can be decorated as we cycle through the exterior edges. Accordingly, we employ a total of $Q-1$ different permutations throughout the whole analog evolution.

Finally, we remark that the complementary case of odd Q can be adapted readily from the even case, if we introduce an additional, auxiliary vertex to the graph. Combining the two cases, we thereby need at most $N_{\text{SWAP}} = Q \left(\frac{Q+1}{2} - 1 \right) = \frac{Q(Q-1)}{2}$ to bridge the Q analog blocks. \square

Meanwhile, analog devices with local qubit connectivities, commonly a nearest-neighbor topology, are also capable of simulating e^{-iG} with a similar resource cost. For nearest-neighbor devices, the identification of the graph Hamiltonian paths [38, 39], for example, enables us to decompose the evolution into $\mathcal{O}(Q)$ analog blocks [40].

IV. ERROR ANALYSIS

Although we have described how to prepare the quantum Hutchinson states $|\chi\rangle$ of Eq. (6) and have bounded the estimate variance arising from the randomness of the state $|\chi\rangle$, it still remains to account for the errors in the measurements of the individual terms of trace estimator $\frac{1}{K} \sum_{k=1}^K \langle \chi_k | A | \chi_k \rangle$, which themselves consist of random and deterministic components.

A. Statistical errors

Let us first assume that the target operator A can be implemented exactly. Let us write out the practical trace estimator, including measurement error, as

$$\mathrm{tr}_K[A] = \frac{1}{K} \sum_{k=1}^K [\langle \chi_k | A | \chi_k \rangle + e_k], \quad (39)$$

where e_k are zero-mean noise contributions independent of the random states. The variance of e_k scales inversely with the shot count N_s for measuring the expectation $\langle \chi_k | A | \chi_k \rangle$.

Meanwhile, the variance of $\frac{1}{K} \sum_{k=1}^K \langle \chi_k | A | \chi_k \rangle$ itself is $\frac{1}{N^2} \sum_{\tilde{m} \neq \tilde{n}} |\langle \tilde{m} | A | \tilde{n} \rangle|^2$ by Eq. (21). It follows that the total variance of our practical trace estimator is

$$\mathbb{V} [\mathrm{tr}_K[A]] = \frac{1}{KN^2} \sum_{\tilde{m} \neq \tilde{n}} |\langle \tilde{m} | A | \tilde{n} \rangle|^2 + \mathcal{O}\left(\frac{1}{KN_s}\right). \quad (40)$$

B. Systematic errors

More realistically, we assume access only to an approximate implementation $\tilde{A} \approx A$ of the target operator. The inexactness generally originates from algorithmic or compilation limitations, including interpolation errors (from the use of spectral filters or accessible operator transformations) and Trotterization errors [41, 42] that result from querying a time evolution $A = e^{-iHt}$, as we will discuss in the next section. Note that here H is different from our quantum Hutchinson Hamiltonian G .

We suppose $\|\tilde{A} - A\|_2 \leq \epsilon$ so that by Weyl's inequality the eigenvalues of \tilde{A} and A are ϵ -close:

$$\max_{0 \leq n \leq N-1} |\tilde{E}_n - E_n| \leq \epsilon. \quad (41)$$

It follows that the normalized traces are also ϵ -close, *i.e.*, $|\mathrm{tr}[\tilde{A}] - \mathrm{tr}[A]| \leq \epsilon$. Hence in this setting our trace estimator has a variance of $\mathbb{V} [\mathrm{tr}_K[\tilde{A}]]$ following Eq. (40) and a bias of at most ϵ .

V. APPLICATIONS

We will consider practical applications to trace estimation of operators that are presented as matrix functions

of a tractable many-body Hamiltonian. We assume a Hamiltonian of the form,

$$H = \sum_{\ell=1}^L \alpha_\ell P_\ell, \quad (42)$$

where $P_\ell \in \mathbb{C}^{N \times N}$ is a Q -qubit Pauli string with weight α_ℓ , and the total number of Pauli strings $L = \mathcal{O}(\mathrm{poly}(Q))$ scales polynomially with the system size. While trace evaluation of the Hamiltonian H itself is straightforward, difficulty arises when we target nonlinear matrix functions of the Hamiltonian, $A = f(H)$.

We focus on two important instances of f , arising respectively from density of states and free energy calculations. For consistency, we let $H = \sum_{n=0}^{N-1} E_n |n\rangle \langle n|$ represent the spectral decomposition of the target Hamiltonian.

A. Density of states

We demonstrate the calculation of density of states for various molecular Hamiltonians in quantum chemistry. The density of states (DOS), $\omega_H(E)$, associated with the target Hamiltonian H is

$$\omega_H(E) = \frac{1}{N} \mathrm{Tr} [\delta(H - E)] = \frac{1}{N} \sum_{n=0}^{N-1} \delta(E_n - E), \quad (43)$$

where $\delta(\cdot)$ is the Dirac delta function. The DOS provides valuable insights into the structure of materials by revealing the energy level distribution and available electronic states. Such information contributes to the understanding of material properties such as electric, optical, and magnetic responses.

We observe that for any normalized state $|\chi\rangle$,

$$\langle \chi | \delta(H - E) | \chi \rangle = \int_{\mathbb{R}} dt \langle \chi | e^{-iHt} | \chi \rangle e^{iEt}, \quad (44)$$

where we have used the Fourier representation of the Dirac delta function. Thus $\omega_H(E)$ can be calculated from the autocorrelation function,

$$s_k(t) = \langle \chi_k | e^{-iHt} | \chi_k \rangle, \quad (45)$$

with respect to sampled quantum Hutchinson states. For short times t , $s_k(t)$ can be efficiently measured using the Hadamard test. When the time t becomes larger, hardware limitations on circuit depth and maximal runtime will ultimately render simulation intractable.

To address this point, we adopt the approach of filter diagonalization [43, 44]. Namely we restrict the effective integration bounds on the RHS of Eq. (44) by introducing a Gaussian filter in the time domain,

$$\int_{\mathbb{R}} dt s_k(t) e^{iEt} \mapsto \frac{1}{\sqrt{2\pi\eta^{-2}}} \int_{\mathbb{R}} dt e^{-\frac{t^2}{2\eta^{-2}}} s_k(t) e^{iEt}, \quad (46)$$

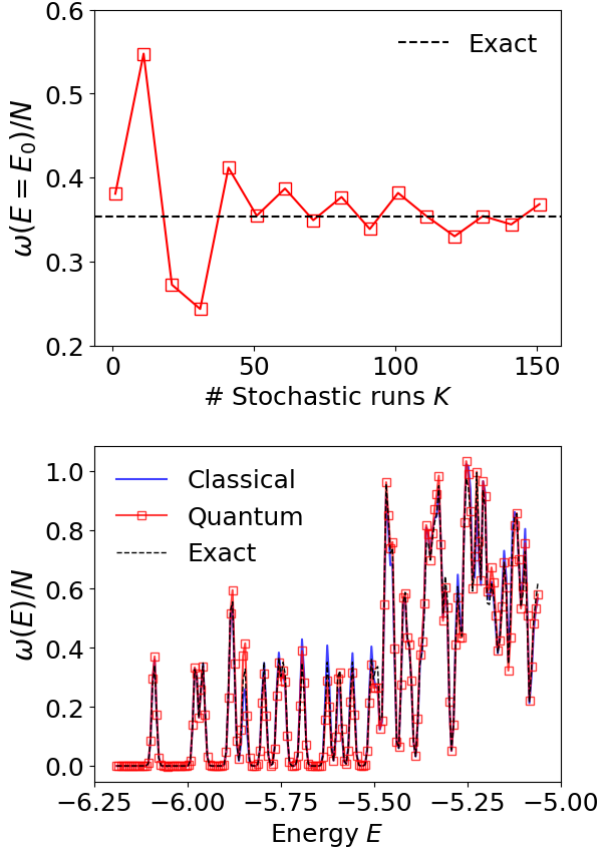


FIG. 5. Density of states (DOS) calculation for the molecular chain of H_6 by the quantum Hutchinson trace estimation. **Top:** DOS at the molecular ground state energy E_0 plotted as a function of the number of quantum Hutchinson states K . Here the DOS is computed with a smearing parameter $\eta = 5.6 \times 10^{-3}$ and explicit access to the operator exponential. The dashed line indicates the exact DOS value. **Bottom:** DOS for $K = 100$ plotted over an energy range encompassing the low-lying part of the spectrum of the molecule. The DOS is evaluated using real-time evolution via Eq. (46) using the trapezoidal rule with time step $\Delta t = 10^{-1}$ and maximal evolution time $t_{\max} = M_{\max} \Delta t = 5 \times 10^2$. The quantum Hutchinson calculation colored in red is compared with classical Hutchinson benchmark colored in blue, where the classical result is obtained assuming explicit access to operator exponential. The relevant energies are reported in units of Hartree.

where η constitutes a small ‘smearing’ parameter. To evaluate Eq. (46), it suffices to consider time evolution for a total duration of $\mathcal{O}(\eta^{-1})$. We will define $\tau_{\text{FD}} := \eta^{-1}$ to be the width of the Gaussian filter in the time domain.

In fact the RHS of Eq. (46) coincides with the smeared DOS:

$$\omega_{H,\eta}(E) = \text{Tr} \left[\frac{1}{\sqrt{2\pi\eta^2}} e^{-(H-E)^2/2\eta^2} \right]. \quad (47)$$

We can calculate the smeared DOS in two ways. First, if we assume direct access to the operator exponential $e^{-(H-E)^2/2\eta^2}$, then we can explicitly evaluate the inner

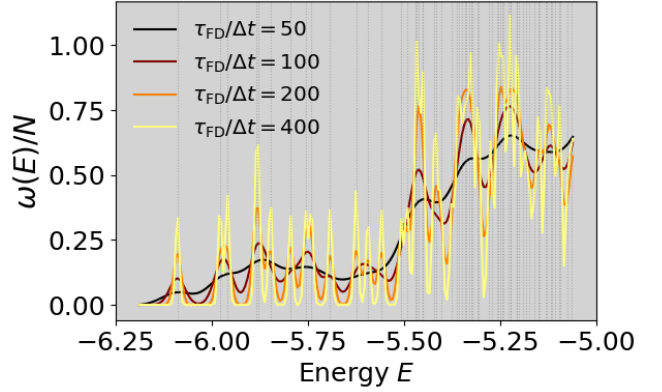


FIG. 6. Density of states (DOS) calculation for the molecular chain H_6 by quantum Hutchinson trace estimation. The DOS profile, constructed with $K = 100$ stochastic runs, is plotted over an energy range encompassing the low-lying eigenenergies of the molecule. The smeared DOS is evaluated following Eq. (46) using real-time evolution e^{-iHt} with time step $\Delta t = 5 \times 10^{-1}$. The quantum Hutchinson calculations are colored according to different choices for the Gaussian filter width $\eta = \tau_{\text{FD}}^{-1}$. The color varies from black (small τ_{FD}) to yellow (large τ_{FD}). Vertical dashed lines in the background indicate the exact molecular eigenenergies. Relevant energies are reported in Hartree units.

product $\langle \chi_k | e^{-(H-E)^2/2\eta^2} | \chi_k \rangle$ using quantum Hutchinson states $|\chi_k\rangle$. Second, we can query the real-time evolution e^{-iHt} to evaluate $s_k(t)$ as defined above and then evaluate the smeared DOS via the RHS of Eq. (46). This real-time evolution approach can be viewed as more native to quantum hardware and illustrates a tradeoff between total evolution time and smearing error.

In Fig. 5, we show the DOS calculation for the molecule H_6 with collinear geometry and bond length 1.5 Å, in an STO-6g basis [45] with 6 orbitals and 6 electrons. The upper panel displays the statistical convergence of the DOS with respect to the number of quantum Hutchinson states. The DOS here is evaluated at $E = E_0$, the molecular ground state energy, and in this calculation we assume direct access to the operator exponential. The typical fluctuation in our estimate diminishes with larger K . Empirically, we observe a reasonable statistical error with $\mathcal{O}(10^2)$ stochastic runs. Fixing $K = 100$, we illustrate in the lower panel the estimated DOS profile across a range of energies E , which encompasses a total of 50 low-lying molecular eigenstates. In contrast to the upper panel, we carry out the DOS evaluation using the real-time approach with Gaussian filter. Using a sufficiently small spectral width η , we observe agreement between the exact and estimated DOS profiles. Moreover, we benchmark against the classical Hutchinson estimation, which gives nearly identical performance.

In the real-time compilation, the maximal evolution time and accordingly the circuit depth are set by the Gaussian width $\tau_{\text{FD}} = \eta^{-1}$. Hence we require fewer quantum resources with a more compact real-time evolution.

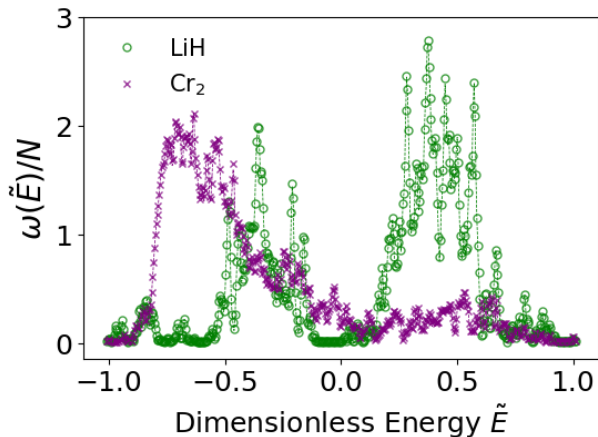


FIG. 7. Density of states (DOS) calculation for molecules LiH and Cr₂ by quantum Hutchinson trace estimation. The DOS profile, constructed with $K = 100$ stochastic runs, is plotted over the dimensionless energy range $\tilde{E} \in [-1, 1]$ by mapping the original spectral range $[E_{\min}, E_{\max}]$ linearly to the interval $[-1, 1]$. The normalized DOS is evaluated as in Eq. (46) using real-time evolution e^{-iHt} with time step $\Delta t = 10^{-1}$ and filter width $\eta = \tau_{\text{FD}}^{-1} = 4 \times 10^{-3}$. Dashed curves indicate the exact DOS with width η . All units are dimensionless.

We show in Fig. 6 a series of DOS profiles constructed with different Gaussian widths. The smeared DOS profile indeed becomes sharply peaked as we extend the width τ_{FD} of the Gaussian window. In practice, we choose the Gaussian filter width mainly based on the thermal energy $\eta \approx k_{\text{B}}T$ of chemical relevance, which in general is much larger than the spacing between adjacent molecular energy levels. Meanwhile for a given τ_{FD} , the choice of the time step Δt determines the frequency at which we query the time evolution operator e^{-iHt_a} where $t_a = a\Delta t$. Consequently, Δt influences the total runtime of the real-time compilation, which is proportional to

$$\sum_{a=1}^{M_{\max}} a\Delta t = \mathcal{O}\left(\frac{\tau_{\text{FD}}^2}{\Delta t}\right), \quad (48)$$

where $M_{\max}\Delta t$ is the maximal evolution time. Note that Δt must be taken sufficiently small to suppress the numerical integration error in Eq. (46). In fact, since the integrand is analytic, the trapezoidal rule converges exponentially fast once $\Delta t \lesssim |E|^{-1}$, *i.e.*, the time step drops below the period of oscillation of the integrand. In Fig. 6, the combination of the Gaussian width $\tau_{\text{FD}} = 10$ and time step $\Delta t = 0.5$ (orange curve) readily captures the major features of the high-resolution DOS profile in Fig. 5.

We remark that the energy spacing of the many-body spectrum typically scales inversely with the dimension N of the Hilbert space. Consequently, the normalized DOS, $\omega_{H,\eta}(E)/N$ (cf. Eq. (47)) for a fixed Gaussian width η , is asymptotically insensitive to the system size. We recall from Eq. (20) that the estimator variance from a single

quantum Hutchinson state can be bounded by above as $\frac{1}{N^2} \sum_{\vec{m} \neq \vec{n}} |\langle \vec{m} | A | \vec{n} \rangle|^2 \leq \frac{1}{N^2} \|A\|_{\text{F}}^2 \leq \frac{1}{N^2} \text{Tr}[A]^2$, where the last inequality holds for any positive semi-definite A . The bound applies in particular to DOS calculations. Hence we may choose the number of quantum Hutchinson states K to be independent of N to achieve comparable statistical errors across molecules of different complexity.

This point is reflected in Fig. 7 for LiH and Cr₂. We treat LiH with the 3-21g basis set [46] (bond length 1.5 Å, 11 orbitals, and 4 electrons). For the Cr₂ dimer known for exhibiting among the strongest electronic correlations, we work with the def2-SVP basis set [47] (bond length 1.5 Å, 30 orbitals, and 24 electrons), and in this calculation only, we restrict our simulation to the widely studied 30-orbital active space, truncating the Hilbert space by considering only a subset of Slater determinants chosen using ASCI [48, 49]. Specifically we choose a truncation dimension of 4000, selected from a one-million determinant ASCI calculation where the 4000 determinants with the largest coefficients are included.

B. Free energy

We turn our attention to free energy calculation for spin systems commonly encountered in condensed matter physics. The free energy encapsulates the entire thermodynamic profile of a many-body system, and it is defined as

$$\mathcal{F}_H = -\beta^{-1} \ln(\text{Tr}[e^{-\beta H}]), \quad (49)$$

where $\beta^{-1} = k_{\text{B}}T$ is the temperature T times the Boltzmann constant k_{B} . The trace in Eq. (49) is known as the partition function \mathcal{Z} .

Applying the continuous functional calculus to the matrix function $f(H) = e^{-\beta H}$, we obtain the following expression for the partition function in terms of the DOS:

$$\mathcal{Z} = \sum_{n=0}^{N-1} e^{-\beta E_n} = \int_{E_{\min}}^{E_{\max}} dE e^{-\beta E} \omega_H(E). \quad (50)$$

Therefore, the partition function (and in turn the free energy) can be computed using our estimator for the DOS introduced in the last section. The accuracy of estimate can be systematically improved by increasing the number K of quantum Hutchinson samples $|\chi_k\rangle$, the width τ_{FD} of time-domain filter, and the number of temporal grid points for which the evolution e^{-iHt} is constructed (*i.e.*, the number of points in our numerical quadrature for Eq. (46)). These parameters do not explicitly depend on the system size, so our quantum algorithm can enjoy computational advantage by avoiding the exponential scaling of Hilbert space. Moreover, the estimation of $\text{Tr}[f(H)]$ for any bounded continuous function $f(\cdot)$ can be performed in the same way.

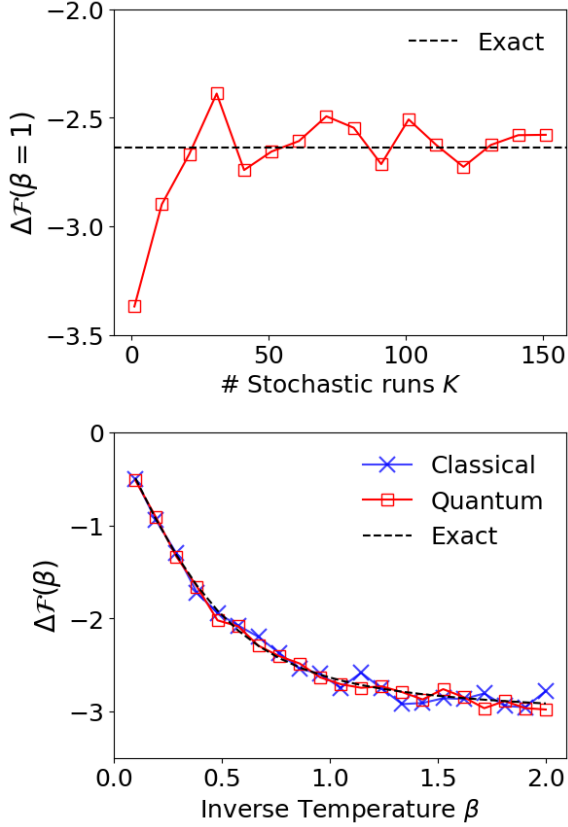


FIG. 8. TFIM free energy calculation for a 1D system of $Q = 8$ spins by quantum Hutchinson trace estimation. The transverse field is varied from $\Omega_{\text{initial}} = 1$ to $\Omega_{\text{final}} = 1.5$. **Top:** Free energy difference at the inverse temperature $\beta = 1$ plotted as a function of the number K of quantum Hutchinson states. The free energy difference, $\Delta\mathcal{F} = -\ln(\text{Tr}[e^{-H_{\text{final}}}] / \text{Tr}[e^{-H_{\text{initial}}}]$), is evaluated assuming explicit access to the operator exponential. Black dashed line marks the exact free energy difference. **Bottom:** Free energy difference for $K = 100$ plotted across a range of temperatures. The free energy difference is evaluated indirectly using the real-time evolution e^{-iHt} with time step $\Delta t = 5 \times 10^{-2}$, maximal evolution time $t_{\text{max}} = M_{\text{max}}\Delta t = 40$, and inverse Gaussian width $\eta^{-1} = \tau_{\text{FD}} = 10$. The quantum Hutchinson calculation colored in red is compared with classical benchmark colored in blue, where the classical estimation is obtained assuming explicit access to operator exponential.

Specifically, we apply our trace estimator to the transverse field Ising model (TFIM),

$$H_{\text{TFIM}} = -J \sum_{i=1}^Q Z_i Z_{i+1} - \Omega \sum_{i=1}^Q X_i, \quad (51)$$

where J controls the spin-spin coupling, Ω determines the transverse field strength, and we adopt the periodic boundary condition $i+Q \equiv i$ on a 1D lattice. As we vary the Hamiltonian parameters (J, Ω) from some initial to final values, we calculate the corresponding difference in the free energy, $\Delta\mathcal{F} = \mathcal{F}_{\text{final}} - \mathcal{F}_{\text{initial}}$.

For our numerical illustration, we fix $J_{\text{initial}} = J_{\text{final}} =$

1 and vary the transverse field Ω from $\Omega_{\text{initial}} = 1$ to $\Omega_{\text{final}} = 1.5$ for a system of $Q = 8$ spins. As in the case of previous DOS calculations, we consider both direct and real-time-based compilation of the operator exponential $e^{-\beta H}$.

We report the results of the free energy calculation for the TFIM chain in Fig. 8. The upper panel demonstrates the statistical convergence of the free energy difference $\Delta\mathcal{F}$ as we increase the number of quantum Hutchinson states, where $\beta = 1$ and we assume direct access to the operator exponential. As expected, the fluctuation in our stochastic estimate decays with K . Fixing a practically effective value of $K = 100$, we display in the lower panel the free energy difference, evaluated using the real-time evolution, across a range of temperatures $0.1 = \beta_{\text{min}} \leq \beta \leq \beta_{\text{max}} = 2$. We observe an excellent agreement among the free energy profiles obtained from the exact, classical Hutchinson, and quantum Hutchinson calculations.

Note that the accuracy of the free energy calculation may be sensitive to the Gaussian width η if the temperature is low. Indeed, if η is not sufficiently small, then the exponential dependence $E \mapsto e^{-\beta E}$ can contribute significant error over the smearing window of width $\mathcal{O}(\eta)$. Therefore we suggest choosing $\eta = \mathcal{O}(\beta^{-1})$ in the low-temperature limit. Observe that computing the DOS to high relative accuracy in the $\eta \rightarrow 0$ limit is more difficult because longer evolution times are required.

C. Thermal expectations

Building on our DOS and free energy discussion, now we delve into the calculation of thermal expectations,

$$\langle O \rangle_H = \frac{\text{Tr}[O e^{-\beta H}]}{\text{Tr}[e^{-\beta H}]} = \frac{\frac{1}{N} \text{Tr}[O e^{-\beta H}]}{\frac{1}{N} \mathcal{Z}}, \quad (52)$$

using a real-time approach. Here O is a Hermitian operator representing a physical observable of interest.

The key quantity to be constructed via quantum measurement is the generalized overlap,

$$s[O](t) = \langle \chi | O e^{-iHt} | \chi \rangle, \quad (53)$$

where $s[O](t) = s(t)$ from Section V A when $O = \mathbb{I}$. In typical applications, such as the computation of the magnetization of a spin system or the 1-RDM of a second-quantized fermionic system, the observable O can be expressed as a linear combination of unitary Pauli strings. Hence, the measurements can be constructed via the corresponding linear combination of Hadamard tests. We can then use these measurements to approximate the following ‘energy-windowed’ trace of the observable:

$$O_{H,\eta}(E) := \text{Tr} \left[O \frac{e^{-(H-E)^2/2\eta^2}}{\sqrt{2\pi\eta^2}} \right], \quad (54)$$

$$= \int_{\mathbb{R}} dt e^{-\frac{t^2}{2\eta^{-2}}} \mathbb{E} s[O](t) e^{iEt}. \quad (55)$$

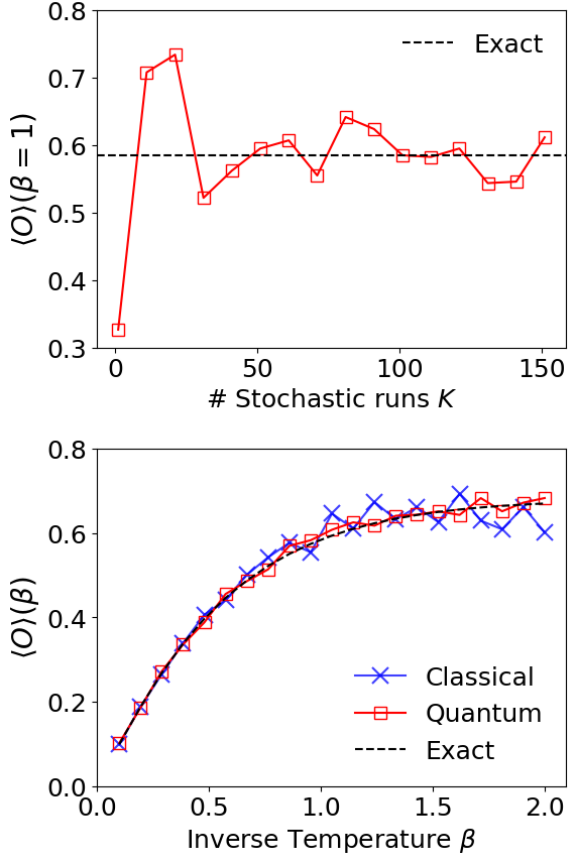


FIG. 9. TFIM adjacent spin-spin correlation calculation for a 1D system of $Q = 8$ spins by quantum Hutchinson trace estimation. The transverse field is fixed at $\Omega = 1$. **Top:** Spin-spin correlation at the inverse temperature $\beta = 1$ plotted as a function of the number K of quantum Hutchinson states. The spin correlation is evaluated assuming explicit access to operator exponential. Black dashed line marks the exact correlation. **Bottom:** Spin-spin correlation for $K = 100$ plotted across a range of temperatures. The correlation is evaluated directly through the real-time evolution e^{-iHt} with time step $\Delta t = 5 \times 10^{-2}$, maximal evolution time $t_{\max} = M_{\max} \Delta t = 40$, and inverse Gaussian width $\eta^{-1} = \tau_{\text{FD}} = 10$. The quantum Hutchinson calculation colored in red is compared with classical benchmark colored in blue, where the classical estimation is obtained assuming explicit access to operator exponential.

By replacing the density operator with its smearing of width η ,

$$e^{-\beta H} \approx \int dE e^{-\beta E} \frac{e^{-(H-E)^2/2\eta^2}}{\sqrt{2\pi\eta^2}}, \quad (56)$$

we obtain the tractable approximation,

$$\frac{\text{Tr}[Oe^{-\beta H}]}{\text{Tr}[e^{-\beta H}]} \approx \frac{\int dE e^{-\beta E} O_{H,\eta}(E)}{\int dE e^{-\beta E} \omega_{H,\eta}(E)}, \quad (57)$$

where expectations in the numerator and of the smeared density of states $\omega_{H,\eta}$ (cf. Eq. (47)) appearing in the denominator can both be estimated empirically using quantum Hutchinson states.

In Fig. 9, we illustrate the real-time approach, as well as a direct approach assuming explicit access to the operator exponential, on the same TFIM chain as in Section VB. Specifically, we fix the observable,

$$O = \frac{1}{Q} \sum_{i=1}^Q Z_i Z_{i+1}, \quad (58)$$

to be the average spin-spin correlation for adjacent spins. In the upper panel of Fig. 9, we show the convergence of the quantum Hutchinson estimator with direct access to the operator exponential. In the lower panel, we demonstrate that the quantum Hutchinson estimator matches the performance of the classical Hutchinson benchmark, using a suitably large number $K = 100$ of Hutchinson states.

D. Implementing non-unitarity

The trace evaluation strategy discussed above exploits the DOS information contained in the temporal evolution of overlap $\langle \chi | e^{-iHt} | \chi \rangle$, where the overlap measurements typically involve the use of a single ancilla qubit [50, 51]. We recall that our real-time trace estimation of a general operator $f(H)$ requires evaluation of the integral,

$$I_k = \int_{\mathbb{R}} dt \hat{f}(t) s_k(t) e^{iEt}, \quad (59)$$

where $\hat{f} : \mathbb{R} \rightarrow \mathbb{C}$ denotes the inverse Fourier transform of the target function f . For each quantum Hutchinson state $|\chi_k\rangle$, the time integral above can then be regarded approximately as a finite sum of Hamiltonian evolutions, *i.e.*, $I_k \approx \langle \chi_k | \sum_{a=1}^M \rho_a e^{-iHt_a} | \chi_k \rangle$. Such a discretization invokes quadrature or importance sampling, both forming linear combination of unitaries (LCU) [15, 52].

Alternatively, we could consider a different emergent class of spectral methods that construct tight polynomial approximations to a broad range of functions of the target Hamiltonian [17, 53, 54]. For example, the quantum eigenvalue transformation of unitary matrices (QET-U) [17] achieves close approximations by querying the controlled forward evolution e^{-iH} , controlled backward evolution e^{iH} , and X -rotations $e^{i\phi X}$ on a single ancilla qubit.

In particular, QET-U can be implemented by a circuit of the form [55]:

$$U_{\text{QET}} = e^{i\phi_0 X} \prod_{\ell=1}^d \left(\mathcal{W}_H e^{i\phi_\ell X} \right), \quad (60)$$

where controlled evolution, $\mathcal{W}_H = |0\rangle\langle 0| \otimes e^{-iH} + |1\rangle\langle 1| \otimes e^{iH}$, acting on the ancilla and system qubits is interlaced

with ancilla X -rotations. The circuit generates a degree- d polynomial approximant,

$$f(H) \approx f_d(H) = \sum_{\ell=0}^{d/2} c_\ell T_{2\ell}(\cos H), \quad (61)$$

where $T_{2\ell}$ denote the even-degree Chebyshev polynomials with associated weights c_ℓ set by the angles $\{\phi_0, \dots, \phi_d\}$. Given an input state $|0\rangle \otimes |\chi\rangle$, the success probability of measuring $|0\rangle$ in ancilla is $\|(\langle 0| \otimes \mathbb{I})U_{\text{QET}}(|0\rangle \otimes |\chi\rangle)\|_2^2 = \langle \chi | f_d^\dagger(H) f_d(H) | \chi \rangle$. For the calculation of the free energy, we recognize $f(H) = e^{-\beta H/2}$ so that

$$\Delta \mathcal{F} \approx -\beta^{-1} \ln \left[\frac{\sum_{k=1}^K \langle \chi_k | f_d(H; \beta)^2 | \chi_k \rangle}{\sum_{k=1}^K \langle \chi_k | f_d(H'; \beta)^2 | \chi_k \rangle} \right]. \quad (62)$$

We remark that LCU and QET-U, as efficient real-time encoding techniques, allow for not only the evaluation of relevant inner products, but also the preparation of the states $f(H)|\chi_k\rangle$. The scope of such state preparation extends well beyond trace estimation; in fact, the use of quantum Hutchinson states yields applications in broader contexts, including accessing general spectral statistics and accelerating elementary matrix operations. Some of these potential applications are discussed in their entirety in Appendices C and D.

VI. CONCLUSION

In this work, we introduce a stochastic trace estimator that is efficiently implementable on quantum hardware. Using real-time evolution under an Ising Hamiltonian that can be conveniently realized on both digital and analog quantum platforms, we construct randomized ‘quantum Hutchinson’ states. These states, combined with real-time strategies for operator encoding, facilitate the approximate trace evaluation of general many-body operators, circumventing the computational cost associated with the exponential Hilbert space scaling. We show that our quantum Hutchinson states match the variance that would be achieved by conventional Hutchinson states in an exponentially high-dimensional space, though the latter can not be realized efficiently with quantum resources. Moreover, we discuss how to implement the real-time estimator with a single reconfigurable circuit whose compilation across different stochastic runs remains unchanged up to modulations in the gate angles. This hardware-adapted implementation is tailored to state-of-the-art digital and analog platforms. While our real-time stochastic estimator can be integrated into a wide variety of tasks beyond trace estimation, we demonstrate applications to density-of-state and free energy calculations essential across the physical, chemical, and materials sciences. The framework presented in this work takes a valuable initial step towards trace estimation compatible with near-term devices and offers novel perspectives on existing approaches.

VII. ACKNOWLEDGMENTS

This work was funded by the U.S. Department of Energy (DOE) under Contract No. DE-AC0205CH11231, through the Office of Science, Office of Advanced Scientific Computing Research (ASCR) Exploratory Research for Extreme-Scale Science (YS, KK, DC, RVB). This research used resources of the National Energy Research Scientific Computing Center (NERSC), a U.S. Department of Energy Office of Science User Facility located at Lawrence Berkeley National Laboratory, operated under Contract No. DE-AC02-05CH11231. ER acknowledges support from the Center for Computational Study of Excited-State Phenomena in Energy Materials (C2SEPEM) at the Lawrence Berkeley National Laboratory, which is funded by the U.S. Department of Energy, Office of Science, Basic Energy Sciences, Materials Sciences and Engineering Division, under Contract No. DE-AC02-05CH11231, as part of the Computational Materials Sciences Program.

APPENDIX

Appendix A: Construction with a single random time

Here we detail the construction, indicated in Section III B, achieving a suitable quantum Hutchinson state with a single random time and a fixed Hamiltonian G .

First, for arbitrary G , consider the full spectral decomposition

$$G = \sum_{n=0}^{N-1} \lambda_n |n^G\rangle \langle n^G|, \quad (A1)$$

with eigenpairs $(\lambda_n, |n^G\rangle)_{n=0}^{N-1}$.

Let us examine the dynamics on an initial state which is a uniform superposition in the G -basis, namely $|\chi^G\rangle := \frac{1}{\sqrt{N}} \sum_{n=0}^{N-1} |n^G\rangle$. For a time $t \in \mathbb{R}$, we denote the corresponding time-evolved state by $|\chi(t)\rangle = e^{-iGt} |\chi^G\rangle$. We will view $|\chi(t)\rangle$ as a random state by randomly sampling *only* the time t from a suitable scalar distribution with probability density $p(t)$. Taking an expectation \mathbb{E} over the time randomness, we arrive at the operator identity,

$$\mathbb{E} [|\chi(t)\rangle \langle \chi(t)|] = \frac{1}{N} \sum_{n,m=0}^{N-1} \mathbb{E} [e^{i(\lambda_n - \lambda_m)t}] |m^G\rangle \langle n^G|, \quad (A2)$$

$$= \frac{1}{N} (\mathbb{I} + \mathbb{B}), \quad (A3)$$

where the operator \mathbb{B} is a bias in the resolution of identity, which we will show can be made zero or extremely small. (Note that in our main construction of Eq. (6), the resolution of identity is always exactly unbiased.)

In the G -basis, \mathbb{B} takes the form,

$$\mathbb{B} = \sum_{n \neq m}^{N-1} \varphi_t(\Delta_{mn}) |m^G\rangle \langle n^G|, \quad (\text{A4})$$

where $\Delta_{mn} = \lambda_n - \lambda_m$ denote the G -eigenvalue differences and $\varphi_t(s) := \mathbb{E}[e^{ist}]$ denotes the characteristic function of the distribution $p(t)$.

A suitable choice of $p(t)$ can effectively control the bias. For example, a Gaussian distribution $p(t) = \frac{1}{\sqrt{2\pi\sigma^2}} e^{-t^2/2\sigma^2}$ yields $\varphi_t(\Delta_{mn}) = e^{-\Delta_{mn}^2\sigma^2/2}$. As σ increases, the bias gets exponentially suppressed. Alternatively, the bias from the fat-tailed distribution $p(t) = \frac{1}{\pi t^2/\sigma} \sin^2(t/\sigma)$ completely vanishes for large σ . In either case, we observe from Eq. (A4) that a nondegenerate G -spectrum, *i.e.*, in which $\Delta_{mn} \neq 0$ for all $m \neq n$, is essential to approximately fulfill the stochastic resolution of identity bias, since indeed $\varphi_t(0) = 1$ always.

In addition to guaranteeing the stochastic resolution of identity, we also want our Hutchinson-type estimator to have an ideal variance. Then for a given operator A whose trace we seek, we can compute the variance of our estimator as:

$$\mathbb{V}[\langle \chi(t) | A | \chi(t) \rangle] = \sum_{m \neq n} \sum_{m' \neq n'} A_{mn}^* A_{m'n'} \varphi_t(\Delta_{m'n'}) \quad (\text{A5})$$

where again the expectation is taken with respect to the distribution $p(t)$ for t and A_{mn} are the matrix elements of A in the G -basis. This variance will match the idealized Hutchinson variance,

$$\sum_{m \neq n} |A_{mn}|^2, \quad (\text{A6})$$

if the all the nontrivial differences of eigenvalue differences, denoted $\Delta_{m'n'}^{mn} = \Delta_{mn} - \Delta_{m'n'}$, where $(m, n) \neq (m', n')$ and $(m, m') \neq (n, n')$, are nonzero and the characteristic function is suitably constructed as outlined above.

To make things more concrete, we consider G which is diagonal in the Z -basis, so $|\chi_0\rangle = |\chi^G\rangle = |+\rangle^{\otimes Q}$. As a first attempt, we use the operator G_1 with an equispaced spectrum $\lambda_n = n$, where $n = 0, \dots, N-1$. In fact G_1 can be tractably constructed on the quantum computer with $Q = \log_2 N$ qubits in terms of the one-qubit number operators as

$$G_1 = \sum_{k=1}^Q 2^{k-1} \Gamma_k. \quad (\text{A7})$$

Although the spectrum of G_1 is nondegenerate, the differences of eigenvalue differences are highly degenerate, hence the variance of the resulting Hutchinson-type estimator is severely suboptimal.

In order to recover performance of the classic Hutchinson estimator, we are motivated to ask: can we find a

simple parametric form of the G -spectrum $\{\lambda_n\}$ such that the resulting ‘excitations’ $\{\Delta_{mn}\}_{m \neq n}$, are all distinct from one another? This same question motivates the theory of Golomb rulers in number theory [56–58].

The simplest explicit specification of a Golomb ruler is the sequence,

$$\lambda_n = Nn^2 + n, \quad 0 \leq n \leq N-1, \quad (\text{A8})$$

where $\min_{m \neq n} |\Delta_{mn}| = \Delta_{01} = N+1$. It is convenient to normalize our sequence of G -eigenvalues, $\lambda_n = \frac{N}{N+1}n^2 + \frac{1}{N+1}n$, so that the minimal excitation is one: $\min_{m \neq n} |\Delta_{mn}| = 1$.

We can construct a Hamiltonian G_2 achieving this spectrum in terms of G_1 :

$$G_2 = \frac{N}{N+1} G_1^2 + \frac{1}{N+1} G_1, \quad (\text{A9})$$

$$= \sum_{i \neq j}^Q h_{ij} Z_i Z_j + \sum_{i=1}^Q h_i Z_i + \text{const.}, \quad (\text{A10})$$

for suitably defined Ising-type interactions h_{ij} and field strengths h_i .

For an appropriate choice of time randomness, *e.g.*, $p(t) = \frac{1}{\pi t^2/\sigma} \sin^2(t/\sigma)$ with $\sigma > 1$, the exact variance of the conventional Hutchinson estimator is therefore recovered.

Note, however, that the parameters h_{ij} and h_i are exponentially large in the number Q of qubits. In order to construct gates implementing time evolution by G of duration t for a random time $t \sim p(t)$, we would need to compute th_{ij} and th_i modulo 2π to high precision. This is in principle possible but would require extended-precision arithmetic as the number of qubits grows. Since time evolution by G would best be achieved by running separate time evolutions by the component terms of the Hamiltonian (whose durations are only significant modulo 2π), we recover an approach similar to our main construction Eq. (6). Although the simplicity of the construction Eq. (6) is to be preferred, it is interesting to observe the connection.

Appendix B: Proof of Lemma 1

Proof. We first note that the matrix identity,

$$\sum_{i=1}^d \vec{m}_i \otimes \vec{m}_i = \sum_{i=1}^d \vec{n}_i \otimes \vec{n}_i, \quad (\text{B1})$$

implies the vector identity,

$$\sum_{i=1}^d \vec{m}_i = \sum_{i=1}^d \vec{n}_i, \quad (\text{B2})$$

when restricted to the diagonal. Therefore in the $d = 1$ case, $\vec{m}_1 = \vec{n}_1$ holds trivially from Eq. (B2).

For the case $d = 2$, we make the following observation based on Eq. (B2): if $\vec{m}_1 = \vec{n}_1$, it must follow that $\vec{m}_2 = \vec{n}_2$. Therefore we can assume that $\vec{m}_1 \neq \vec{n}_1$, and it remains only to show that $\vec{m}_1 = \vec{n}_2$ or $\vec{n}_1 = \vec{m}_2$, because then in either case Eq. (B2) then immediately implies $(\vec{m}_1, \vec{m}_2) = (\vec{n}_2, \vec{n}_1)$.

By the assumption $\vec{m}_1 \neq \vec{n}_1$, there exists an index $a \in \{1, \dots, Q\}$ such that either $(m_{1,a}, n_{1,a}) = (0, 1)$ or $(m_{1,a}, n_{1,a}) = (1, 0)$. In these respective cases, Eq. (B2) implies the component identity $(m_{2,a}, n_{2,a}) = (1, 0)$ or $(m_{2,a}, n_{2,a}) = (0, 1)$, respectively. Taking the a -th column of Eq. (B1), we obtain

$$m_{1,a}\vec{m}_1 + m_{2,a}\vec{m}_2 = n_{1,a}\vec{n}_1 + n_{2,a}\vec{n}_2. \quad (\text{B3})$$

Therefore we must have either $\vec{n}_1 = \vec{m}_2$ or $\vec{m}_1 = \vec{n}_2$, as was to be shown.

Finally we turn to the case $d = 3$, where we can apply our previous results inductively. First observe that if $\vec{m}_1 = \vec{n}_1$, then by Eq. (B1) and our proof in the case $d = 2$, it follows that $(\vec{m}_2, \vec{m}_3) = \mathcal{P}_2(\vec{n}_2, \vec{n}_3)$ for a suitable permutation \mathcal{P}_2 .

Therefore we can assume that $\vec{m}_1 \neq \vec{n}_1$, so there exists $a \in \{1, \dots, Q\}$ such that $(m_{1,a}, n_{1,a}) = (0, 1)$ or $(m_{1,a}, n_{1,a}) = (1, 0)$. Without loss of generality, we focus on the case $(m_{1,a}, n_{1,a}) = (1, 0)$, since similar arguments hold for the complementary case $(m_{1,a}, n_{1,a}) = (0, 1)$ due to the binary symmetry.

The a -th component of the vector identity Eq. (B2) then reads as

$$1 + m_{2,a} + m_{3,a} = n_{2,a} + n_{3,a}. \quad (\text{B4})$$

Among $m_{2,a}, m_{3,a}, n_{2,a}, n_{3,a} \in \{0, 1\}$, this equation is solved only by the following choices:

$$(m_{2,a}, m_{3,a}, n_{2,a}, n_{3,a}) = \begin{cases} (0, 0, 1, 0) \\ (0, 0, 0, 1) \\ (1, 0, 1, 1) \\ (0, 1, 1, 1) \end{cases}. \quad (\text{B5})$$

Then once again taking the a -th column of Eq. (B1), observe that the first two cases imply $\vec{m}_1 = \vec{n}_2$ and $\vec{m}_1 = \vec{n}_3$, respectively. Either way, we can again reduce to the case $d = 2$.

Then it remains only to consider the last two cases in Eq. (B5). Taking the a -th column of Eq. (B1), these two cases imply that $\vec{m}_1 + \vec{m}_2 = \vec{n}_2 + \vec{n}_3$ and $\vec{m}_1 + \vec{m}_3 = \vec{n}_2 + \vec{n}_3$, respectively. But then by Eq. (B2), we must have either $\vec{m}_3 = \vec{n}_1$ or $\vec{m}_2 = \vec{n}_1$, respectively. Either way, we can finally once again reduce to the case $d = 2$, and the proof is complete.

We remark that these combinatorial arguments do not hold when $d \geq 4$ because the list of cases analogous to Eq. (B5) fails to allow us to reduce to the cases $d \leq 3$. \square

Appendix C: Spectral statistics beyond trace

Consider the problem of estimating the spectral moments $\frac{1}{N} \sum_{n=0}^{N-1} |f(E_n)|^q$, of a target operator $A = f(H)$, where q is a positive integer. In the special case $q = 2$, we recover the squared Frobenius norm of the target operator,

$$\frac{1}{N} \sum_{n=0}^{N-1} |f(E_n)|^2 = \frac{1}{N} \text{Tr}[A^\dagger A] = \frac{1}{N} \|A\|_F^2, \quad (\text{C1})$$

up to a normalization.

Following Eq. (C1), our quantum Hutchinson trace estimator can be applied to the operator $B = A^\dagger A$, yielding $\frac{1}{N} \|A\|_F^2 = \mathbb{E} \langle \chi | B | \chi \rangle$.

Here real-time approaches for the matrix function can be adapted readily using either the LCU or QET-U approach from Section VD, given an approximate compilation of $A = f(H)$. LCU involves the evaluation of the expectations $\langle \chi_k | \sum_{a < b} \rho_a^* \rho_b e^{-iH(t_a - t_b)} | \chi_k \rangle$, while QET-U measures the vector norms $\langle \chi_k | f_d^\dagger(H) f_d(H) | \chi_k \rangle$.

The general case $q \geq 2$ corresponds furnishes the normalized Schatten norm of the target operator:

$$\frac{1}{N} \sum_{n=0}^{N-1} |f(E_n)|^q = \frac{1}{N} \text{Tr}[|A|^q] = \frac{1}{N} \|A\|_{S,q}^q, \quad (\text{C2})$$

where $|A| = \sqrt{A^\dagger A}$. When q is an even integer, we observe that the normalized Schatten norm can be evaluated as above through an LCU or QET-U compilation of A .

Appendix D: Fast matrix computations

In addition to trace and spectral moment calculations, elementary matrix operations can also be accelerated using quantum Hutchinson states. For example, let us consider the multiplication $A = f(H)g^\dagger(H)$ of two matrix functions f and g . This matrix product can be compressed stochastically using the resolution of identity:

$$\frac{1}{N} A = \mathbb{E} [|f_\chi\rangle \langle g_\chi|], \quad (\text{D1})$$

where we define $|f_\chi\rangle = f(H)|\chi\rangle$ and $|g_\chi\rangle = g(H)|\chi\rangle$ for quantum Hutchinson states $|\chi\rangle$.

The stochastic resolution of identity allows for efficient preparation of the state $A|\psi\rangle$ via

$$\frac{1}{N} A|\psi\rangle \approx \sum_{k=1}^K \langle g_{\chi,k} | \psi \rangle |f_{\chi,k}\rangle. \quad (\text{D2})$$

Observe that Eq. (D2) suggests an LCU formula for the desired state preparation. Here the insertion of a stochastic resolution of identity effectively splits the state preparation process into two pieces that separately query $f(H)$ and $g(H)$.

- [1] D. Chandler, *Introduction to Modern Statistical Mechanics* (Oxford University Press, 1987).
- [2] H. Rue and L. Held, *Gaussian Markov random fields: theory and applications* (CRC press, 2005).
- [3] I. Han, D. Malioutov, and J. Shin, in *Proceedings of the 32nd International Conference on Machine Learning*, Proceedings of Machine Learning Research, Vol. 37, edited by F. Bach and D. Blei (PMLR, Lille, France, 2015) pp. 908–917.
- [4] E. Di Napoli, E. Polizzi, and Y. Saad, *Numerical Linear Algebra with Applications* **23**, 674 (2016).
- [5] L. Lin, Y. Saad, and C. Yang, *SIAM Review* **58**, 34 (2016).
- [6] T. Q. Chen, Y. Rubanova, J. Bettencourt, and D. K. Duvenaud, in *Neural Information Processing Systems* (2018).
- [7] R. Baer, D. Neuhauser, and E. Rabani, *Annual Review of Physical Chemistry* **73**, 255 (2022), pMID: 35081326.
- [8] P. R. Halmos, *The Annals of Mathematical Statistics* **17**, 34 (1946).
- [9] M. Hutchinson, *Communications in Statistics - Simulation and Computation* **19**, 433 (1990).
- [10] R. N. Silver and H. Röder, *Phys. Rev. E* **56**, 4822 (1997).
- [11] T. Itaka and T. Ebisuzaki, *Phys. Rev. E* **69**, 057701 (2004).
- [12] H. Avron and S. Toledo, *J. ACM* **58**, 10.1145/1944345.1944349 (2011).
- [13] R. A. Meyer, C. Musco, C. Musco, and D. P. Woodruff, *Symposium on Simplicity in Algorithms (SOSA)*, , 142 (2021).
- [14] E. N. Epperly, J. A. Tropp, and R. J. Webber, arXiv preprint arXiv:2301.07825 <https://doi.org/10.48550/arXiv.2301.07825> (2023).
- [15] A. Childs and N. Wiebe, *Quantum Information and Computation* **12** (2012).
- [16] G. H. Low and I. L. Chuang, *Phys. Rev. Lett.* **118**, 010501 (2017).
- [17] Y. Dong, L. Lin, and Y. Tong, *PRX Quantum* **3**, 040305 (2022).
- [18] A. Girard, *Numerische Mathematik* **56**, 1 (1989).
- [19] E. Knill and R. Laflamme, *Phys. Rev. Lett.* **81**, 5672 (1998).
- [20] S. Goto, R. Kaneko, and I. Danshita, *Phys. Rev. B* **104**, 045133 (2021).
- [21] S. Goto, R. Kaneko, and I. Danshita, *Phys. Rev. B* **107**, 024307 (2023).
- [22] N. Keenan, N. F. Robertson, T. Murphy, S. Zhuk, and J. Goold, *npj Quantum Information* **9**, 72 (2023).
- [23] H. Wang, J. Nan, T. Zhang, X. Qiu, W. Chen, and X. Li, *Phys. Rev. B* **108**, 085102 (2023).
- [24] A. Summer, C. Chiaracane, M. T. Mitchison, and J. Goold [10.48550/arXiv.2303.13476](https://arxiv.org/abs/2303.13476) (2023), arXiv:2303.13476 [quant-ph].
- [25] S. Bravyi, A. Chowdhury, D. Gosset, and P. Wocjan, arXiv preprint arXiv:2110.15466 <https://doi.org/10.48550/arXiv.2110.15466> (2021).
- [26] Y. Nakata and M. Mura, *International Journal of Quantum Information* **11**, 1350062 (2013).
- [27] Y. Nakata, M. Koashi, and M. Mura, *New Journal of Physics* **16**, 053043 (2014).
- [28] M. Motta, C. Sun, A. T. Tan, M. J. O’Rourke, E. Ye, A. J. Minnich, F. G. Brandão, and G. K.-L. Chan, *Nat. Phys.* **16**, 205 (2020).
- [29] S. R. White, *Phys. Rev. Lett.* **102**, 190601 (2009).
- [30] R. V. Mishmash, T. P. Gujarati, M. Motta, H. Zhai, G. K.-L. Chan, and A. Mezzacapo, *Journal of Chemical Theory and Computation* **19**, 3194 (2023), pMID: 37227024.
- [31] J. Spencer, *Journal of Combinatorial Theory* **5**, 1 (1968).
- [32] E. F. Assmus and J. D. Key, *Designs and their Codes*, Cambridge Tracts in Mathematics (Cambridge University Press, 1992).
- [33] T. Feder and C. S. Subi (2012).
- [34] H. Bernien, S. Schwartz, A. Keesling, H. Levine, A. Omran, H. Pichler, S. Choi, A. S. Zibrov, M. Endres, M. Greiner, V. Vuletić, and M. D. Lukin, *Nature* **551**, 579 (2017).
- [35] D. Bluvstein, H. Levine, G. Semeghini, T. T. Wang, S. Ebadi, M. Kalinowski, A. Keesling, N. Maskara, H. Pichler, M. Greiner, V. Vuletić, and M. D. Lukin, *Nature* **604**, 451 (2022).
- [36] Z. Baranyai, *Infinite and finite sets* (1974).
- [37] *Topics in Chromatic Graph Theory*, Encyclopedia of Mathematics and its Applications (Cambridge University Press, 2015).
- [38] B. Alspach, J.-C. Bermond, and D. Sotteau, *Decomposition into cycles i: Hamilton decompositions*, in *Cycles and Rays* (Springer Netherlands, Dordrecht, 1990) pp. 9–18.
- [39] R. Glebov, Z. Luria, and B. Sudakov, *Israel Journal of Mathematics* **222**, 91 (2017).
- [40] A. Galicia, B. Ramon, E. Solano, and M. Sanz, *Phys. Rev. Res.* **2**, 033103 (2020).
- [41] S. Lloyd, *Science* **273**, 1073 (1996).
- [42] A. M. Childs, Y. Su, M. C. Tran, N. Wiebe, and S. Zhu, *Phys. Rev. X* **11**, 011020 (2021).
- [43] M. R. Wall and D. Neuhauser, *The Journal of Chemical Physics* **102**, 8011 (1995).
- [44] A. Schuckert, A. Bohrdt, E. Crane, and M. Knap, *Phys. Rev. B* **107**, L140410 (2023).
- [45] W. J. Hehre, R. F. Stewart, and J. A. Pople, *J. Chem. Phys.* **51**, 2657 (1969).
- [46] J. S. Binkley, J. A. Pople, and W. J. Hehre, *Journal of the American Chemical Society* **102**, 939 (1980).
- [47] F. Weigend and R. Ahlrichs, *Physical Chemistry Chemical Physics* **7**, 3297 (2005).
- [48] N. M. Tubman, J. Lee, T. Y. Takeshita, M. Head-Gordon, and K. B. Whaley, *J. Chem. Phys.* **145**, 044112 (2016).
- [49] N. M. Tubman, C. D. Freeman, D. S. Levine, D. Hait, M. Head-Gordon, and K. B. Whaley, *J. Chem. Theory Comput.* **16**, 2139 (2020).
- [50] R. Cleve, A. Ekert, C. Macchiavello, and M. Mosca, *Proc. Roy. Soc. Lond. A* **454**, 339 (1998), arXiv:quant-ph/9708016.
- [51] C. L. Cortes and S. K. Gray, *Phys. Rev. A* **105**, 022417 (2022).
- [52] S. Chakraborty [10.48550/arXiv.2302.13555](https://arxiv.org/abs/2302.13555) (2023), arXiv:2302.13555 [quant-ph].
- [53] A. Gilyén, Y. Su, G. H. Low, and N. Wiebe (Association for Computing Machinery, New York, NY, USA, 2019).
- [54] D. Motlagh and N. Wiebe,

- arXiv preprint arXiv:2308.01501
<https://doi.org/10.48550/arXiv.2308.01501> (2023).
- [55] H. H. S. Chan, D. M. Ramo, and N. Fitzpatrick, arXiv preprint arXiv:2303.06161 <https://doi.org/10.48550/arXiv.2303.06161> (2023).
- [56] S. Sidon, *Mathematische Annalen* **106**, 536 (1932).
- [57] S. W. Golomb, Academic Press, New York **23**, 37 (1972).
- [58] K. Drakakis, *Advances in Mathematics of Communications* **3**, 235 (2009).